

*Third International Symposium on the Effects of Surface Geology on Seismic Motion
Grenoble, France, 30 August - 1 September 2006
Paper Number: xxx*

Numerical Benchmark: Seismic Modeling Trials Using E3D with the ModelAssembler Community Modeling Environment

John N. Louie¹

1 Nevada Seismological Laboratory, University of Nevada, Reno, USA; louie@seismo.unr.edu

ABSTRACT - The ModelAssembler community seismic modeling environment (CME) is adapted to the ESG Grenoble numerical benchmark tests. The CME, meant to be a tool for those who are not computational specialists, assembles disparate scales of geologic and geophysical data into the 3D grids needed by Larsen's E3D finite-difference code. Predicted ground shaking was computed to 60 seconds at 1.0 Hz maximum frequency on a desktop workstation. Infinite Q and no free-surface topography were applied throughout. Maps of maximum ground velocity show basin amplification factors of 2-20, and a lack of obvious correlation between amplification and basin depth or dip of the basin floor. Animations of shaking show strong trapping and long shaking durations in the basin. Amplification patterns within the basin suggest the prominent effects of scenario-dependent geometric phenomena such as fault-rupture directivity and refraction through a lens-shaped basin floor. Efforts to increase model realism could include lower surface velocities in bedrock, lateral velocity heterogeneities within the basin and bedrock, the true extent of the Grenoble basin, and many of the other neighboring basins; as well as topography.

1. Introduction

These computations in response to the 2006 ESG numerical benchmark challenge employed Shawn Larsen's E3D code (Larsen et al., 2001) from Lawrence Livermore National Laboratory (LLNL), USA. E3D is listed by the OECD's Nuclear Energy Agency at <http://www.nea.fr/abs/html/ests1300.html>. This code was most recently vetted at the March 24-25, 2004 Next Generation Attenuation (NGA) Workshop as part of the Pacific Earthquake Engineering Research Center (PEER)/Southern California Earthquake Center (SCEC) 3D Ground Motion Project Team led by S. Day. Larsen had also participated in the 3D Modeling Workshop sponsored by N. Abrahamson and SCEC held in Santa Ana, Calif., October 2-3, 1997. Work with E3D on 3-d modeling and synthetics for the San Francisco Bay region was published by Stidham et al. (1999). Larsen's E3D computation platform has proven to be a reliable seismic synthetic generator for more than a decade.

My participation in the numerical benchmark is not intended to test or vet the E3D program. I have not made any alterations to Larsen's E3D compute engine itself. Rather, my intention is to benchmark the combination of E3D with my ModelAssembler Community Seismic Modeling Environment (CME). ModelAssembler is an open-source, Java-based velocity-model gridding code that can integrate scattered and heterogeneous geophysical data sets. It also provides facilities for visualizing model grids and computed results as maps, cross sections, and movies. Source code for ModelAssembler is available from <http://www.seismo.unr.edu/geothermal/#ma>.

The concept of a Community Modeling Environment (CME) was developed at SCEC under U.S. National Science Foundation Information Technology Research sponsorship. SCEC's CME combines, in part, geologically based 3D velocity and fault databases, developed as consensus models in the regional geophysical community (e.g., Magistrale et al., 2000), with a seismic-modeling computational engine (e.g., Olsen, 2000). The innovation of SCEC's velocity model is that it is expressed not as a preset 3D grid but as flexible computer code, able to create grids of various extents and node spacings. This innovation simplifies the process of creating high-resolution grids for local modeling, or geographically extensive grids with larger spacings for large-area but low-frequency models. (The finer the grid spacing, the higher the frequencies that can be modeled.)

My purpose in creating ModelAssembler was initially to provide a community velocity model and seismic modeling environment for Nevada urban areas, with funding from the U.S. Dept. of Energy, Lawrence Livermore National Laboratory and the Geothermal Technologies Program. Reno and Las Vegas are subject to earthquake hazards both from below their local basins, and from faults up to 200 km away. Thus, attacking the problems of modeling scenario events, or modeling small events for which ground-motion data have been recorded, demand running synthetic seismograms for a wide variety of models on a spectrum of scales.

S. Larsen of LLNL assisted me tremendously in creating a Nevada CME by training my group in the use of E3D and installing it on facilities in the Nevada Seismological Lab. Pancha et al. (2004) modeled recorded ground motions in the Reno-area basin from an earthquake in 2000, 60 km west of the basin. Louie et al. (2005) modeled the complex surface-wave interactions of the regional basins surrounding the Las Vegas basin, and separating it from a 1992 earthquake 100 km to the west. More recently, the process of extending ModelAssembler to render the model of Benites and Olsen (2005) for Wellington, New Zealand, and for this Grenoble numerical benchmark, have allowed me to improve its flexibility. I hope to make seismic modeling tools such as E3D available to seismologists and earthquake engineers in general, where to date such tools have mostly been available to specialists in computational geophysics.

So it is not my intention to benchmark new developments in earthquake ground-motion computation. Instead, I hope to benchmark a new general availability of seismic modeling to a wider group of users. I do not expect that my benchmark results will show any technical or computational breakthroughs in the prediction of earthquake ground motions. I do hope that my results may show that an adequately accurate 3D ground-motion estimation tool is now available to a wide user base.

2. Methods

ModelAssembler is essentially a pre-processor for E3D, and is run in advance of E3D. MA accepts geographic (latitude and longitude) locations for sources and receivers, and reads geological and geophysical data files. MA outputs 3D grids of P velocity, shear velocity, and density, along with a control file for E3D. E3D can then be run directly on the MA outputs. The geological and geophysical data files input are all in readable text format, specify properties at points located with geographic coordinates, and do not rely on the data having any particular sorting or organization. Edits and additions to the data files are easy to make.

Fundamental to ModelAssembler is the concept that low-resolution regional data sets can be superimposed by detailed local data sets (Louie et al., 2005). Grids at any scale can thus be created as composites of various results at very different scales. In Nevada, a

data set with the depths of sedimentary and volcanic basins sampled at 2 km spacing is often combined with local datasets from the urban basins that sample basin depth at 0.4 km spacing. Geotechnical data sets are also incorporated, despite having spacings varying between 0.1 and 0.3 km, and including isolated point measurements. MA interpolates all the disparate data sets onto the regular grid requested, following instructions for how one data set may take precedence over another where they overlap.

ModelAssembler makes use primarily of two geological/geophysical data sets to create the 3D velocity and density grids: Neogene basin depths; and geotechnical measurements of shallow shear velocities. For a surface grid node located in a basin, MA interpolates the basin data given, using the precedence instructed, to find a Neogene basin thickness for that node. Geological data can be consulted if the user wishes to distinguish between volcanic-filled and sediment-filled Neogene basins.

Each model is accompanied by a set of rules governing how the interpolations are done, how geophysical properties will vary with depth inside and outside basins, and how the properties not supplied in the data sets will be estimated from the ones that are supplied. Thus in bedrock outside basins in most areas the rules describe a P-velocity versus depth profile $V_p(z)$, and equations for estimating the corresponding shear velocity V_s and density ρ . In Nevada the basin $\rho(z)$ profile is assumed (from oil-field measurements) and V_p and V_s are estimated. Thus at present MA yields laterally homogeneous properties within basin and bedrock, although the interface between basin and bedrock can vary wildly in depth. For this Grenoble numerical benchmark, the organizers supplied laterally homogeneous basin and bedrock profiles of V_p , V_s , and density as well as a basin depth map with 0.25-km sampling.

Lateral variation in grid properties within a basin, or within bedrock, is only allowed near the surface with ModelAssembler at present. In the Wellington model, for example, the 0.1-km-thick surface zone has its velocities adjusted when a node is within an adjustable radius of a location where shear velocities have been measured. Along that radius the average shear velocity to 30 m depth, V_{s30} , grades from an assumed value to the measured V_{s30} value at the point. In Wellington, Benites and Olsen (2005) assumed $V_{s30}=0.175$ km/s in basins and $V_{s30}=1.5$ km/s in bedrock. MA then forms a weighted average by slowness of the V_{s30} value and the shear velocities between 0.03 and 0.1 km depth, for a 0.1-km-thick upper grid zone. If bedrock shallows to within the thickness of the upper grid zone, then the weighted slowness average also includes the thickness of bedrock, with its corresponding velocity, that is within the depth of the upper zone.

Figure 1 shows maps of Grenoble basin geophysical properties supplied for the computational benchmark, as gridded at 0.1-km resolution and rendered by ModelAssembler. At left is a shaded-relief map of bedrock elevation, showing the surface below which shear velocity is greater than 2.0 km/s, including the depth of the Grenoble basin from Vallon (1999). In the benchmark the basin is artificially terminated at its one southern and two northern extremities. The green-blue transition is at sea level and the surrounding mountains rise above 2 km elevation (white). Free-surface topography is shown for geographic reference only and is *not* included in these computations.

Subsurface basin topography *is* included. Circles on Fig. 1 indicate two complexities in basin geometry, spots where the bedrock is shallower than the 0.1-km upper-zone thickness. At right is a map showing the shear velocity of the upper zone of the computation grid, 0.1 km thick. Velocities in this zone rise when $V_s=3.2$ km/s bedrock (dark blue color) is at less than 0.1 km depth, producing shear velocities of 0.45-0.85 km/s (yellow color in circles and at basin edges in Fig. 1 at right) by slowness-averaging. Where bedrock is deeper than 0.1 km, the benchmark model describes $V_s=0.34$ km/s (orange color) throughout the surface of the basin.

Using the grids produced by ModelAssembler, I computed a map of maximum ground velocity and 40 three-component velocity time-histories for each of the four benchmark event specifications, designated W1, W2, S1, and S2. The E3D computation grid had 400 zones north-south, 350 zones east-west, and 63 zones in depth, at a grid spacing of 0.1 km in all directions. The grids extended only to 6.2 km depth since the supplied model of bedrock properties had a constant velocity from 3 to 27 km depth, and all sources were in the upper 4.5 km. A time step of 0.008 s was employed to meet the Courant condition.

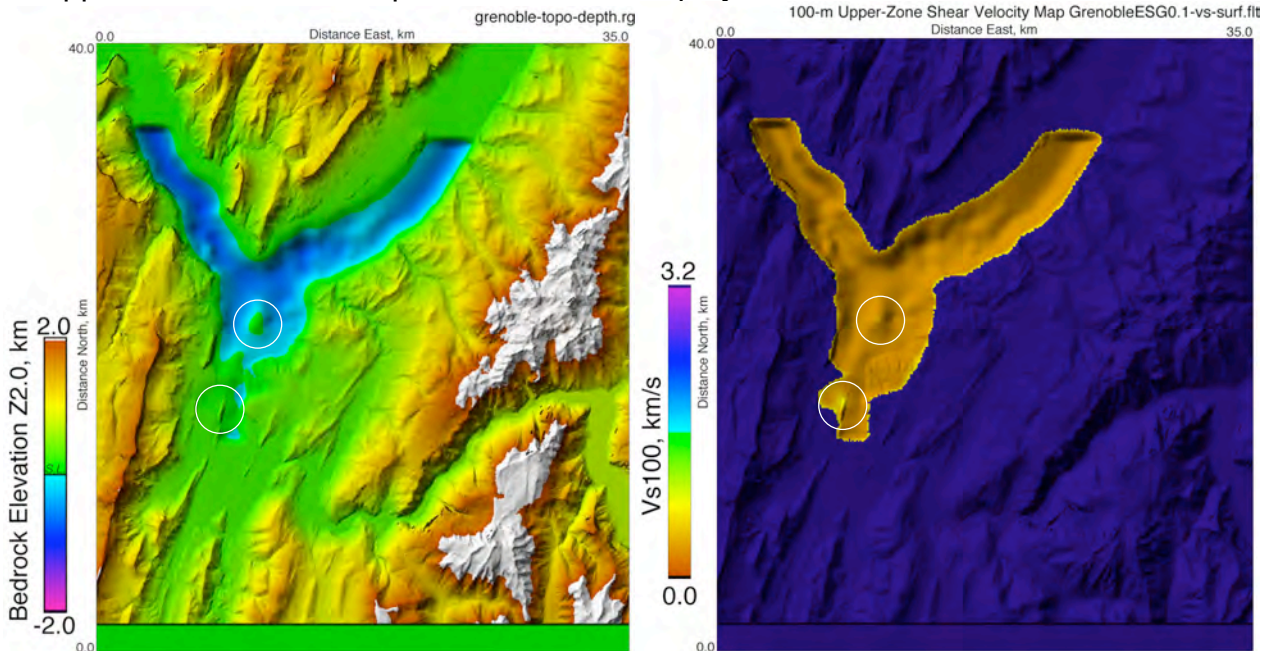


Figure 1. Maps of Grenoble basin geophysical properties as rendered by ModelAssembler for the benchmark runs on E3D. At left is a shaded-relief map of bedrock elevation; at right is a map showing the shear velocity of the upper zone of the computation grid, 0.1 km thick. Sea level is at the blue-green color transition on the left. Circles indicate areas where bedrock shallows to less than 0.1 km depth, raising the averaged surface-zone velocity. Free-surface topography is shown for geographic reference only and is not included in the computations. (Topographic data were not supplied for the green strip on the south side of the model at left.) Subsurface basin topography is included.

The computations required about 225 Mb of RAM for E3D, and the four runs were completed in a total of about 36 hours on a desktop SunBlade 1500 with the UltraSparc architecture and SunOS 5.9. Thus these results did not require the parallel computing capabilities of E3D, or the use of the Collaboratory for Computational Geosciences (CCoG) cluster (www.seismo.unr.edu/ccog) or the Nevada Environmental Computing Grid (NECG; aces.dri.edu). ModelAssembler and E3D have been configured to use the CCoG and NECG grid facilities for problems requiring up to 30 Gb RAM.

However, my response to this benchmark challenge is to show what is feasible on anyone's desktop. The results here have frequencies up to 1.0 Hz. The limits on the grid properties as set up by ModelAssembler are listed in Table I. These are as specified for the benchmark.

With a minimum velocity of 0.32 km/s, the 0.1-km grid spacing does not strictly avoid grid dispersion at 1.0 Hz. The minimum wavelength is 0.32 km, sampled by only three 0.1-km grid intervals instead of the five required (Larsen et al., 2001). The minimum velocity exists in the rendered grid only in the surface zones within the basin. Careful inspection of animations of the modeled wave propagation (available from <http://www.seismo.unr.edu/hazsurv/Grenoble/>) failed to show any waves propagating at

erroneous lower velocities, or any “pincushion” distortion of circular wavefronts. It seems likely that any grid dispersion may have lengthened the predicted shaking durations at 1.0 Hz, but not materially so.

Grid Limits	
min V_p	1.45 km/s
max V_p	5.92 km/s
min V_s	0.32 km/s
max V_s	3.43 km/s
min ρ	1.91 g/cm ³
max ρ	2.72 g/cm ³

Table I. Extreme values of Grenoble benchmark model grid properties.

Some differences from the benchmark specifications are listed below. These differences are not due to any limitations in the E3D code. They are due to limits at present in ModelAssembler, or due to my desire to provide results that could be computed quickly on anyone's desktop:

- a) Q is infinite everywhere, instead of a finite Q being used in the basin.
- b) The derivative of the source time-function used I used was a Ricker wavelet, rather than the Gaussian that would have been the derivative of the specified source time-function, an error function.
- c) All my results use no free-surface topography. My results do include the full 3D representations of the basin-bottom and fault geometries that were provided.

As Figure 1 shows in yellow on the right, the shallow parts of the basin floor provide some gradational lateral variations in the shear velocity of the upper zone.

3. Results

Synthetic seismograms submitted by benchmark participants will be compared at the ESG conference and are not shown here. My computed ground-velocity maps show many interesting features that can be examined in this paper. Figure 2 shows maps of maximum horizontal ground velocity computed at 1.0 Hz by E3D over the assembled Grenoble model for the benchmark M2.8-M2.9 “weak” events W1 (left side) and W2 (right side). Source W1 is a right-lateral strike-slip point double-couple source 3 km below the surface representing a fault-plane strike of N45°E and dip of 90° (Fig. 2, left). The quadrupolar pattern of strong shaking is apparent above the sources in bedrock, with both events' point double couples exhibiting the expected small nodal motions in the directions 45° away from their P and T axes.

Overall, maximum ground velocities at 1.0 Hz are amplified within the Grenoble basin by factors of 2 to 20 over motions in adjacent bedrock. Corners of the basin most distant from the sources show maximum ground velocities that are 60 times amplified relative to the velocities in adjacent bedrock. The shaded-relief of basin-floor topography behind the maximum ground-velocity colors suggests there is no correlation between basin depth and amplification. Neither do the highest amplifications generally appear over the steepest walls of the basin. Instead, the patterns of amplification in Figure 2 may be heavily dependent on the relative location of portions of the basin with respect to the source radiation pattern, and thus on the exact earthquake scenario.

Animations of ground-motion snapshots (not shown) indicate strong conversion to and trapping of surface-wave energy within the basin, with shaking lasting beyond the 60 sec

computed. The ratio of ground velocities inside versus outside the basin increases during at least the first 30 sec of the simulation.

A strong basin-edge effect is apparent in Figure 2 (left side) on the basin's steeply dipping northeast boundary, where shear waves radiating from the nearby point double couple (normal to the fault plane) convert to surface waves in the basin. Over the next 30 seconds these trapped surface waves diffuse slowly (at about 0.32 km/s) into the remainder of the basin, though less strongly into the more distant northwest arm of the basin.

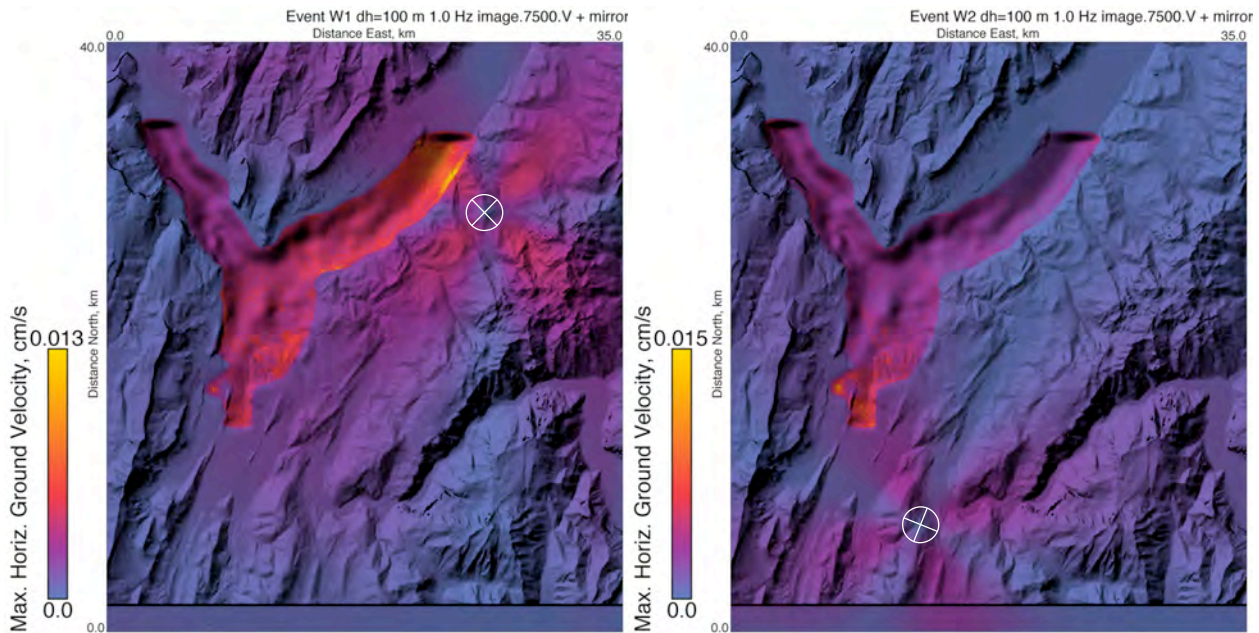


Figure 2. Maps of maximum horizontal ground velocity computed at 1.0 Hz by E3D over the assembled Grenoble model for benchmark “weak” events W1 (left) and W2 (right). Free-surface topography shown for geographic reference only. Stronger maximum ground velocities are represented by orange and yellow colors, scaled to the individual maximum of each map.

Source W2 is a left-lateral strike-slip point double couple 3 km deep representing a N60°W strike and 90° dip fault. W2 is farther from the southern tip of the basin, which is shallower than the northeast part, with more gently sloping sides. So the converted basin phases from W2 are weaker than they are for W1. Ground motions within the basin decrease away from the source, but amplifications relative to adjacent bedrock motions remain in the range of 2-20 times, occasionally larger.

Figure 3 shows time-slice maps of E3D-computed ground shaking for the benchmark M6.0 finite-fault “strong” events S1 and S2. Each rupture initiates at the center of its fault trace 3.0 km below the surface, and propagates at 2.8 km/s to fill the fault area with a constant final slip of 1.116 m. The rectangular faults extend from the surface to 4.5 km depth and are 9.0 km long. The S1 fault strikes N45°E and the S2 fault strikes N60°W; both dip at 90°. E3D imposes a point source at each grid node intersected by the fault. Thus a total moment of 1.356×10^{25} dyne-cm (for the specified 1.116 meter of slip) is divided up, for S1, among 65 nodes horizontally times 46 nodes vertically— 2990 nodes in all that each act as a point double-couple source when triggered. S2, which despite having the same fault length, with a more westerly strike lies across 79 nodes horizontally, for a total of 3634 node-point sources.

The time-slices (Fig. 3) and animations of the finite-fault models are striking for the strong waves that appear as effects of fault-rupture directivity (animations of the wave

propagation from all four sources can be downloaded from <http://www.seismo.unr.edu/hazsurv/Grenoble/>). Since rupture initiates below the center of each fault in the benchmark tests, the strong shaking due to rupture directivity propagates from both ends of the fault, in the general direction of fault strike. The strong waves resulting from S1's rupture directivity toward the southwest are labeled with "D" in Figure 3 (left side). Such waves also appear at the lower right corner of Figure 3 (right side).

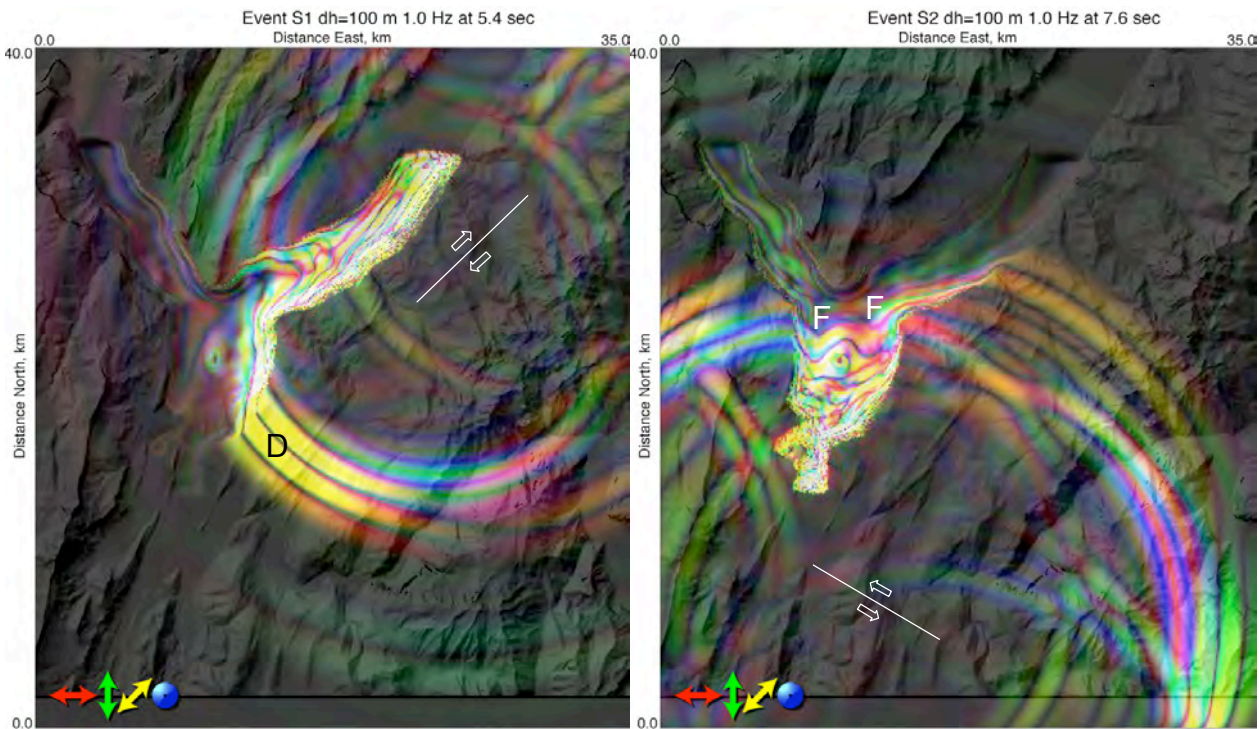


Figure 3. Time-slice maps of ground shaking for the benchmark events S1 (left, at 5.4 sec after rupture initiation) and S2 (right, at 7.6 sec after rupture initiation). Colors are keyed to ground-motion polarizations as indicated at the lower left, with brighter colors indicating higher ground-motion velocities. Thus a bright purple indicates large velocities on both the east-west and up-down components for example, combining red and blue colors. S1's rupture directivity toward the southwest is labeled with "D." S2's focusing wavefronts are indicated on the right with "F"s. Topography is shown for geographic reference only. Animations from all four sources can be downloaded from <http://www.seismo.unr.edu/hazsurv/Grenoble/>.

Shear waves from S2, refracting up from the basin floor and bent by its concave shape into focusing, concave wavefronts are indicated on the right with "F"s. These geometric focusing effects are clearest where velocities do not vary laterally, except across the basin boundaries, as in this benchmark model. Lateral velocity heterogeneities in the bedrock or basin would scatter and disperse the amplification peaks resulting from rupture directivity and basin-bottom refraction.

Figure 4 shows the maps of maximum horizontal ground velocity computed for S1 (left) and S2 (right). The southwestward directivity of S1 has induced greater shaking along the southeast edge of the basin on the left, much different from the pattern of weak motions in Fig. 4 (left) for the small W1 event. In particular, the finite-fault rupture shows a bipolar source radiation pattern, due to rupture directivity, instead of the quadrupolar pattern of the point double-couple W1 source. Thus the highest shaking in the basin is on its southeastern rather than its northeastern edge, where the directivity-induced waves hit the basin.

The Grenoble basin is not in the path of the S2 rupture's directivity (Fig. 4, right), so is not as excited by S2 as it is to S1. The ground-velocity color scale is normalized on the right to a higher maximum shaking of 1.464 cm/s instead of the 1.028 cm/s on the left, so its colors appear darker. If plotted on the same scale, both events would show the same radiation patterns in bedrock (though rotated). The heightened shaking from S2 appears only in a small, lens-shaped side basin (arrow in Fig. 4, right) just 900 m wide and 91 m deep. This amplification of a very small area may be due to geometric focusing, as in the diffraction caustic observed in Santa Monica from the 1994 Northridge, Calif. Earthquake by Husker et al. (2006).

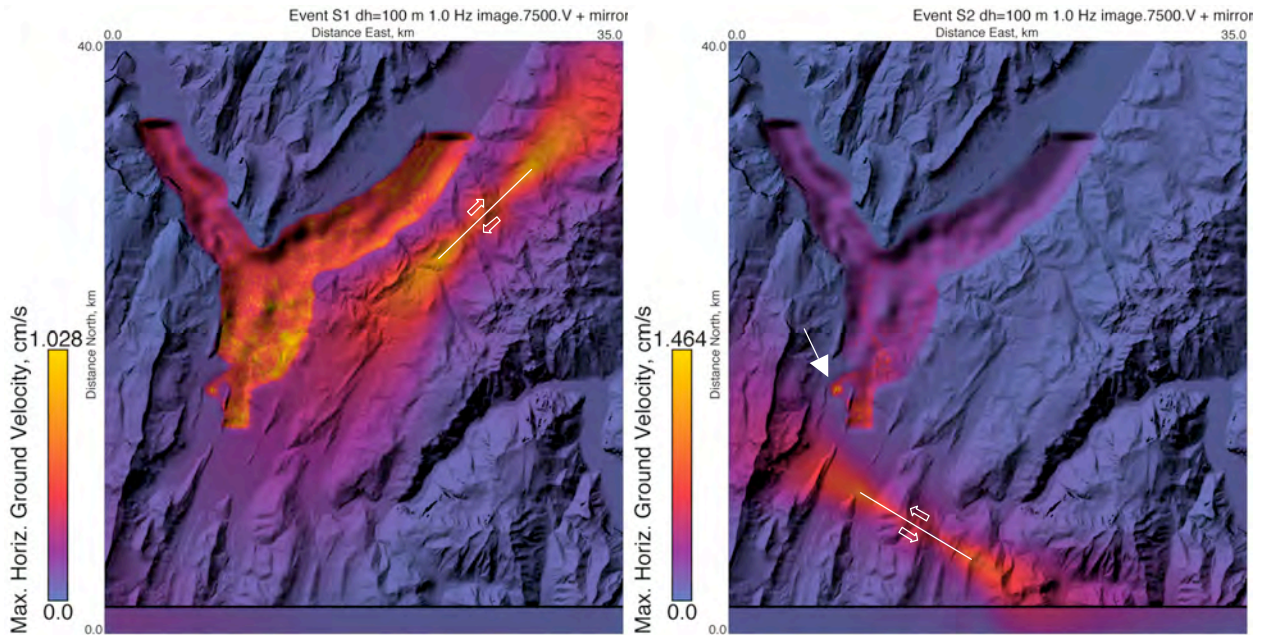


Figure 4. Maps of maximum horizontal ground velocity computed at 1.0 Hz by E3D over the assembled Grenoble model for benchmark M6.0 finite-fault events S1 (left) and S2 (right). Topography is shown for geographic reference only. The southwestward directivity of S1 has induced greater shaking along the southeast edge of the basin on the left. The ground-velocity color scale is normalized on the right to 1.464 cm/s instead of 1.028 cm/s on the left, so its colors appear darker. The heightened shaking from S2 appears only in a small side basin (arrow).

4. Discussion

The maximum ground velocities of about 1.0 cm/s computed for the “strong” events S1 and S2 (Figure 4) seem too small considering the close proximity of the Grenoble basin, and the 6.0 magnitude of the events. The (spectral) PGA at 1 Hz would be only 1 cm/s^2 or $0.1\% g$. The maximum motion on each side of the fault planes should be 50 cm/s, but at the surface E3D appears to be showing lower velocities of grid-node volumes that are averaging over 0.1-km-cubed regions. It is possible that I have made an error in describing the sources to E3D. If this were the case, for this entirely linear computation, multiplying all ground velocities by a constant factor would correct them precisely. Thus any ground-motion ratio or amplification factor computed from these results should be correct despite any such error, whether between sites, spectral, or over time.

The minimal ground shaking may also have arisen partly as a result of aspects of the benchmark basin model that are, I feel, simplifications of aspects of the true geophysical setting. These aspects may well be important to accurate modeling of ground motions in

Grenoble, and have proved important in other areas. Such model simplifications are, of course, in addition to the many other simplifications employed here that could affect seismic waves at their sources, or at recording sites. I did not explore any of these in a free-style prediction attempt, however.

The most prominent of these simplified aspects is the benchmark model's continuation of 3.2 km/s shear velocity right to the surface in bedrock. Extensive campaigns measuring shallow shear velocity at hundreds of sites are summarized by Scott et al. (2004) and Thelen et al. (2006 in press), and further results are posted at <http://www.seismo.unr.edu/vs/archive/> and can be interactively mapped at <http://mapserver.library.unr.edu/website/seismoweb/VS30/viewer.htm>.

Shallow shear velocities measured on even the most competent bedrock in Nevada, California, and New Zealand show V_{s30} values only rarely as high as 1.0 km/s. These lower velocities tend to be present only within 20-50 m of the surface, since V_{s100} values over bedrock are much higher. Comparison tests placing such a low-velocity channel at the surface in bedrock areas of the Wellington model of Benites and Olsen (2005) suggest the presence of the channel almost doubles maximum ground motions in the basins, not just in the bedrock. Energy from events occurring below bedrock areas is trapped in the surface channel, converted to surface waves, and propagates into the basins. Without the channel, much energy simply reflects from the free surface and propagates down and out of the model. Adding lower surface velocities in bedrock areas of the Grenoble model should result in higher predicted ground motions.

Other possibly unrealistic aspects of the benchmark model are: the laterally constant velocities within basins and within bedrock; the artificial termination of the Grenoble basin at its northern and southern extremes; and the existence of the Grenoble basin in isolation, with none of the other basins in the region that surrounds it. Scott et al. (2004, 2006) and Thelen et al. (2006) show the high degree of variation in V_{s30} that exists in the alluvial basins of Reno, Las Vegas, and San Gabriel Valley. V_{s30} shows fractal statistics and can vary by a factor of two over 0.3 km distances due to variations in alluvial sediment grain size and soil development. Stochastic media trap and amplify seismic energy more efficiently than any laterally homogeneous media (Frankel and Wennerberg, 1987). Great variations in shallow shear velocities have also been noted in bedrock by Wald et al. (2004), which often correlate well with topographic slope.

The artificial termination of the Grenoble basin traps energy that in the real basin might bleed out the ends of the basin up- and down-river. Louie et al. (2005) observed strong conversion of energy within distant basins that diffuses additional shaking very late into the Las Vegas basin, for models of the urban basin set among the dozens of other basins in southern Nevada.

5. Conclusions

The ModelAssembler community seismic modeling environment (CME) has been successfully adapted to the ESG Grenoble numerical benchmark tests. The CME assembles disparate scales of geologic and geophysical data into the 3D grids needed by Larsen's E3D finite-difference seismic modeling code. Predicted ground shaking was computed to 60 seconds at 1.0 Hz maximum frequency on a desktop workstation. The maximum-shaking maps show basin amplification factors of 2-20, and a lack of obvious correlation between amplification and basin depth or dip of the basin floor. Animations of shaking show strong trapping and long shaking durations in the basin. Amplification patterns within the basin suggest the prominent effects of scenario-dependent geometric

phenomena such as fault-rupture directivity and refraction through a lens-shaped basin floor. More realistic model grids could include lower surface velocities in bedrock, lateral velocity heterogeneities within the basin and bedrock, the true extent of the Grenoble basin, and many of the other neighboring basins; as well as topography.

6. References

- Benites, R., and K. B. Olsen (2005). Modeling strong ground motion in the Wellington metropolitan area, New Zealand. *Bulletin of the Seismological Society of America* 95, 2180–2196.
- Frankel, A., and Wennerberg, L. G. (1987). Energy-flux model of seismic coda; separation of scattering and intrinsic attenuation. *Bulletin of the Seismological Society of America* 77, 1223-1251.
- Husker, A. L., Kohler, M. D., and Davis, P. M. (2006). Anomalous seismic amplitudes measured in the Los Angeles Basin interpreted as a basin-edge diffraction catastrophe. *Bulletin of the Seismological Society of America* 96, 47-164.
- Larsen, S., Wiley, R., Roberts, P., and House, L. (2001). Next-generation numerical modeling: incorporating elasticity, anisotropy and attenuation. Society of Exploration Geophysicists Annual International Meeting, *Expanded Abstracts*, 1218-1221.
- Louie, J. N., Pancha, A., Biasi, G. P., Heimgartner, M., Coolbaugh, M. F., and Larsen, S. (2005). Tests and applications of 3-d geophysical model assembly in the Great Basin. *Seismological Society of America Annual Meeting*, April 26-29, Lake Tahoe, Nevada.
- Magistrale, H., S. Day, R. W. Clayton, and R. Graves (2000). The SCEC Southern California Reference Three-Dimensional Seismic Velocity Model Version 2. *Bulletin of the Seismological Society of America* 90(6B), S65–S76.
- Olsen, K. B. (2000).. Site amplification in the Los Angeles Basin from three-dimensional modeling of ground motion. *Bulletin of the Seismological Society of America* 90(6B), S77-S94.
- Pancha, A., J. G. Anderson, J. N. Louie, A. AnooShehpoor, and G. Biasi (2004). Data and simulation of ground motion for Reno, Nevada. *Proceedings of the 13th World Conf. on Earthquake Engineering*, Vancouver, B.C., Aug. 1-6, paper no. 3452.
- Scott, J. B., M. Clark, T. Rennie, A. Pancha, H. Park and J. N. Louie (2004). A shallow shear-wave velocity transect across the Reno, Nevada area basin. *Bulletin of the Seismological Society of America* 94, 2222-2228.
- Scott, J. B., T. Rasmussen, B. Luke, W. Taylor, J. L. Wagoner, S. B. Smith, and J. N. Louie (2006 in press). Shallow shear velocity and seismic microzonation of the urban Las Vegas, Nevada basin. *Bulletin of the Seismological Society of America* 96(3), June.
- Stidham, C., Antolik, M., Dreger, D., Larsen, S., Romanowicz, B. (1999). Three-dimensional structure influences on the strong-motion wavefield of the 1989 Loma Prieta earthquake. *Bulletin of the Seismological Society of America* 89, 1187-1202.
- Thelen, W. A., M. Clark, C. T. Lopez, C. Loughner, H. Park, J. B. Scott, S. B. Smith, B. Greschke, and J. N. Louie (2006 in press). A transect of 200 shallow shear velocity profiles across the Los Angeles Basin. *Bulletin of the Seismological Society of America* 96(3), June.
- Vallon, M. (1999). Estimation de l'épaisseur d'alluvions et sédiments Quaternaires dans la région Grenobloise par inversion des anomalies gravimétriques. LGGE, Université Joseph Fourier, IPSN/CNRS (in French), 33 pp.
- Wald, D. J., Earle, P. S., and Quitoriano, V. (2004). Topographic slope as a proxy for seismic site amplification correction. *Eos Trans. AGU* 85(47), Fall Meet. Suppl., Abstract S42A-01.

6.1 Locations of supplementary electronic media

<http://www.seismo.unr.edu/hazsurv/Grenoble/> lists movie files (in full resolution and in MPEG-4 for video iPods), full-resolution graphic files, and the 20.7-Mb “ESGBench-Louie3D.tar” archive with the requested benchmark results.

<http://www.seismo.unr.edu/geothermal/#ma> allows general access to ModelAssembler source code, geophysical data files for Nevada, and student exercises with MA and E3D.